Stability of a Rayleigh-Bénard poiseuille flow for yield stress fluids - Comparison between Bingham and regularized models

Christel Métivier, Chérif Nouar

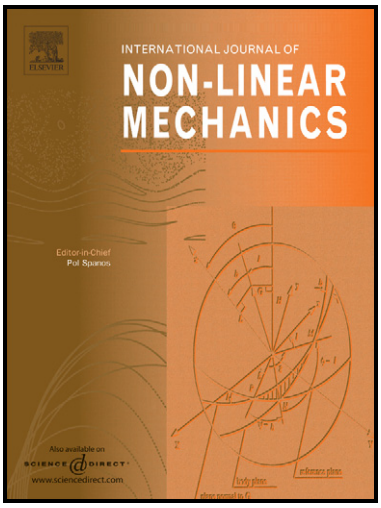

www.elsevier.com/locate/nlm

Stability of a Rayleigh-Bénard poiseuille flow for yield stress fluids - Comparison between Bingham and regularized models

Christel Métivier, Chérif Nouar

PII: S0020-7462(11)00144-2
DOI: doi:10.1016/j.ijnonlinmec.2011.05.017
Reference: NLM 1886

To appear in: *International Journal of Non-Linear Mechanics*

Received date: 5 May 2010
Revised date: 6 December 2010
Accepted date: 27 May 2011

Cite this article as: Christel Métivier and Chérif Nouar, Stability of a Rayleigh-Bénard poiseuille flow for yield stress fluids - Comparison between Bingham and regularized models, *International Journal of Non-Linear Mechanics*, doi:10.1016/j.ijnonlinmec.2011.05.017

Stability of a Rayleigh-Bénard Poiseuille flow for yield stress fluids - Comparison between Bingham and regularized models

Christel Métivier[a], Chérif Nouar[b]

[a]*Laboratoire de Rhéologie, UMR 5520 (UJF - CNRS - Grenoble INP)*
Tel.: +33-476825179
christel.metivier@ujf-grenoble.fr
[b]*LEMTA, UMR 7563 (CNRS - INPL - UHP)*
cherif.nouar@ensem.inpl-nancy.fr

Abstract

A linear stability analysis of a Rayleigh-Bénard Poiseuille flow is performed for yield stress fluids whether we use the Bingham or regularized models. A fundamental difference between those models is that the effective viscosity is not defined in the plug zone for the Bingham model, while it is defined in the whole domain for the regularized models. For these models, the viscosity depends highly on a parameter ε near the axis and increases drastically in an intermediate region. The convergence of the critical conditions between the simple and the Bingham models is not obtained. However, we show that the Bercovier and Papanastasiou models can tend to the exact Bingham results.

Keywords: Fluid mechanics, linear stability, yield stress fluids

1. Introduction

Different models are used in the literature to describe a yield stress fluid. The simplest one is the Bingham model. It is commonly used to describe the rheological behaviour of a large range of fluids as muds of drilling for instance. It assumes that the material moves as a rigid solid prior to yielding and behaves as a viscous fluid afterwards. By definintion, the sol-gel transition for a Bingham fluid is not continuous in terms of material behaviour. The "gel-like" region, called plug or unyielded zone, and the "liquid-like" region are separated by a distinct yield surface. Furthermore, except few

simple configurations [1], the determination of the yield surface location is the major difficulty in the numerical resolution of the Bingham fluid flow. To avoid these limitations, several authors use regularized models. These models consider a viscous behaviour in the whole flow domain and replace the unyielded zone by an extremely viscous fluid past a transition in the shear rate. The aim of our study is to compare the different models and show the relevance of using either regularized models or Bingham model in a particular situation: stability problems. In this paper, we investigate the Rayleigh-Bénard Poiseuille (RBP) flow for yield stress fluids. This configuration has already been studied for a Bingham fluid in [2] and [3] performing linear stability analyses.

On the other hand, the usage of regularized models in stability analysis has been studied recently by [4] and [5]. In [4], the authors treat a linearly stable flow: the plane Poiseuille flow of a Bingham fluid. The authors show that the regularized models can exhibit spurious behaviour and can give rise to unstable eigenmodes. The eigenvalues are called spurious in the sense that they depend on the small parameter introduced in the regularized model. These values can be detected by varying the number of nodes in calculations. In [5], the linear stability of the circular Couette flow of viscoplastic fluid leads to critical conditions for both the Bingham and a regularized models. The author indicates that the regularization has practically no influence on critical conditions. Actually, it is not surprising that in the case of plane Poiseuille flow, the regularized model leads to an instability at finite Reynolds number. Indeed, replacing a rigid plug zone by a highly viscous zone (whatever, the large value of the viscosity, i.e. the small is the regularization parameter), leads to a problem fundamentally different from that of a true plane Bingham Poiseuille flow. However, it is not clear in Frigaard and Nouar [4] how the critical conditions depend on the regularization model and on the regularization parameter. The analysis of the viscosity profiles combined with the work of Govindarajan *et al.* [6] where it is shown that the critical conditions depend mainly on the viscosity stratification in the critical layer (region where the energy of fluctuations is produced by interactions with the mean flow), may lead to the conclusion that the critical conditions are mainly independent on the regularization parameter, when it is sufficiently small.

In the case of the Taylor Couette problem, where the instability is driven by the centrifugal force, it can be understood that here, replacing a rigid solid (if it exists) by a hyghly viscous zone could be equivalent. Here, we want

to clarify this point by considering an other situation. In this respect, we propose to consider the linear stability of the RBP flow involving a yield stress fluid whether a Bingham or regularized models are used. The framework of this study concerns dominant buoyancy-driven source of instability compared to the shear-driven one, i.e. we consider weak Reynolds values. In outline, our paper proceeds as follows. In Section 2, the basic state of the RBP flow is given for the Bingham model and the regularized models. A comparison between the different models is performed. The linear stability analysis is developed in § 3. The numerical results are presented in Section 4 as well as a comparison between the viscoplastic models.

2. Fully developed Rayleigh-Bénard Poiseuille flow

We consider the plane Poiseuille flow of a yield stress fluid between two horizontal walls separeted by a distance L. The system of coordinates as well as the shape of the axial velocity component are represented on Fig.(1). As classical, we assume that the lower wall is heated at temperature $T_0 + \delta T/2$ while the upper wall is at $T_0 - \delta T/2$. Using the Boussinesq approximation, the problem is governed by the following equations:

$$\boldsymbol{\nabla} \cdot \boldsymbol{U} = 0\,, \tag{1}$$

$$Re\,\boldsymbol{U}_t + Re^2\,Pr\,(\boldsymbol{U}\cdot\boldsymbol{\nabla})\,\boldsymbol{U} + \boldsymbol{\nabla}P - RaT\,\boldsymbol{e}_y - Re\,Pr\boldsymbol{\nabla}\cdot\boldsymbol{\tau} = 0\,, \tag{2}$$

$$T_t + Pr\,Re\,(\boldsymbol{U}\cdot\boldsymbol{\nabla})\,T - \nabla^2 T = 0\,. \tag{3}$$

They are rendered in dimensionless form using the centerline velocity U_0 as velocity scale, the width L of the plane channel as lengthscale, then $(\mu_0 U_0)/L$ as stress scale, the thermal diffusion time L^2/a between the two walls as time scale, where a is the thermal diffusivity, and $(\mu_0 a)/L^2$ as the pressure scale. The modified temperature is used $T = \dfrac{T - T_0}{\delta T}$.

The Reynolds Re, the Prandtl Pr, and the Rayleigh Ra numbers are defined by: $Re = \dfrac{\rho\,U_0 L}{\mu_0}$, $Pr = \dfrac{\mu_0}{a\rho}$ and $Ra = \dfrac{g\rho\,\beta\,\delta T L^3}{\mu_0 a}$. $\boldsymbol{U}$ is the velocity field, p the pressure field, $\boldsymbol{\tau}$ the deviatoric stress tensor, T the temperature, ρ the density, β the thermal expansion and $\boldsymbol{g}$ the gravitational acceleration. The velocity vector $\boldsymbol{U}$ is of the form $\boldsymbol{U} = U\,\boldsymbol{e}_{\mathrm{x}} + \mathrm{V}\,\boldsymbol{e}_{\mathrm{y}} + \mathrm{W}\,\boldsymbol{e}_{\mathrm{z}}$, where U, V, W are the velocity components and $\boldsymbol{e}_{\mathrm{x}}, \boldsymbol{e}_{\mathrm{y}}, \boldsymbol{e}_{\mathrm{z}}$ are unit vectors in the streamwise x, transversal y and spanwise z directions respectively. We write the no-slip and imposed temperature conditions at the walls as follows:

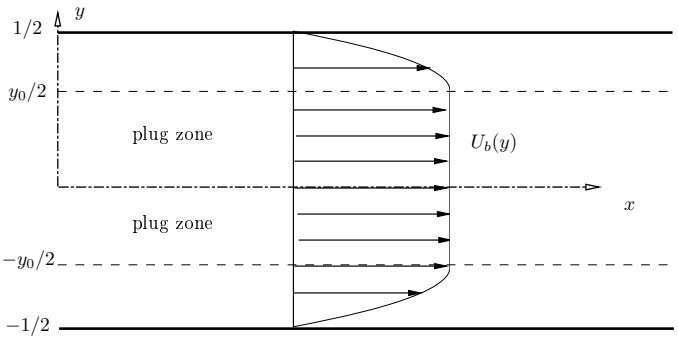

Figure 1: Fully developed Poiseuille flow for a yield stress fluid

$\boldsymbol{U}(\pm 1/2) = \mathbf{0}$ and
$T(1/2) = -1/2$, $T(-1/2) = 1/2$.

2.1. Bingham model

Employing the von Mises yield criterion, the Bingham model, in dimensionless form can be written [1]:

$$\boldsymbol{\tau} = \mu \dot{\boldsymbol{\gamma}} \qquad \text{if} \quad \tau > \mathrm{B}\,, \tag{4}$$

$$\dot{\gamma} = 0 \qquad \text{if} \quad \tau \leq B\,. \tag{5}$$

The parameter μ represents the effective viscosity and is defined by :
$\mu = 1 + \dfrac{B}{\dot{\gamma}}$, where $B = \tau_0 L/(\mu_0 U_0)$, is the Bingham number. The second invariant of the rate of strain tensor $\dot{\boldsymbol{\gamma}}$ and that of the deviatoric stress tensor are respectively $\dot{\gamma}$ and τ.

Equations (1)-(3) are satisfied in the whole flow domain. However, in the region where the yield stress is not exceeded, the rate of strain tensor is identically zero. This region moves then as a rigid solid and is called plug zone. The interface separating the "liquid like" and the "gel like" domains is a yield surface and is defined by the criterion $\tau = B$, then $\dot{\gamma} = 0$.

For a one dimensional shear flow and fully developed thermal field, we have $V = W = 0$ and $U_B = U_B(y)$:

$$U_B(y) = \begin{cases} 1 & ; \qquad |y| \leq \frac{1}{2} y_0\,, \\ 1 - \left(\dfrac{2\,|y| \,-\, y_0}{1 - y_0} \right)^2 & ; \qquad \frac{1}{2} y_0 <\mid y \mid< \frac{1}{2}\,, \end{cases} \tag{6}$$

$T_b = \dfrac{T_0}{\delta T} - 2y$ and $P_b\,(x,y) \;=\; P_0 - Ra\,y^2 - 8\dfrac{Re\,Pr}{(1-y_0)^2}\,x$, with $\pm\,(1/2)\;y_0$, the position of the yield surfaces. The velocity of the basic flow depends only on B. The relation between y_0 and B is given by: $(2y_0-1)^2 B - 4y_0 = 0$.

2.2. regularized models

In this paper, we consider three models which are commonly used in the literature:
Simple model with a regularized parameter, for example used by Beris *et al.* [7]:

$$\boldsymbol{\tau} = \mu_s \dot{\boldsymbol{\gamma}}_{\boldsymbol{s}} = \left(1 + B\left(\frac{1}{\dot{\gamma}_s + \varepsilon}\right)\right)\dot{\boldsymbol{\gamma}}_{\boldsymbol{s}} = \left(1 + B\,F_s\left(\dot{\gamma}_s, \varepsilon\right)\right)\dot{\boldsymbol{\gamma}}_{\boldsymbol{s}}\,. \tag{7}$$

Papanastasiou model [8]:

$$\boldsymbol{\tau} = \mu_p \dot{\boldsymbol{\gamma}}_{\boldsymbol{p}} = \left(1 + B\left(\frac{1 - e^{-\frac{\dot{\gamma}_p}{\varepsilon}}}{\dot{\gamma}_p}\right)\right)\dot{\boldsymbol{\gamma}}_{\boldsymbol{p}} = \left(1 + B\,F_p\left(\dot{\gamma}_p, \varepsilon\right)\right)\dot{\boldsymbol{\gamma}}_{\boldsymbol{p}}\,. \tag{8}$$

Bercovier model [9] :

$$\boldsymbol{\tau} = \mu_{be} \dot{\boldsymbol{\gamma}}_{\boldsymbol{be}} = \left(1 + B\left(\frac{1}{\sqrt{\dot{\gamma}_{be}{}^2 + \varepsilon^2}}\right)\right)\dot{\boldsymbol{\gamma}}_{\boldsymbol{be}} = \left(1 + B\,F_{be}\left(\dot{\gamma}_{be}, \varepsilon\right)\right)\dot{\boldsymbol{\gamma}}_{\boldsymbol{be}}\,, \tag{9}$$

μ_s, μ_p and μ_{be} represent the effective viscosity for each model respectively. Here the Bingham model is recovered when the parameter ε tends to zero.

The velocity profile of the fully developed flow is completely defined by Eqs. (2) and (7), (8) or (9). For a unidirectional shear flow, $U_{reg}(y)$ satisfies:

$$\left(\frac{2B}{y_0}\right) y = \left(1 + B\,F\right) DU_{reg}\,, \tag{10}$$

with $D = \dfrac{d}{dy}$. The velocity profile is determined numerically using finite difference scheme.

2.3. Comparison between the different models

This section compares the main characteristics of the basic flow whether the Bingham or the regularized models are used. For the axial velocity profiles, the numerical results indicate that the convergence is verified when

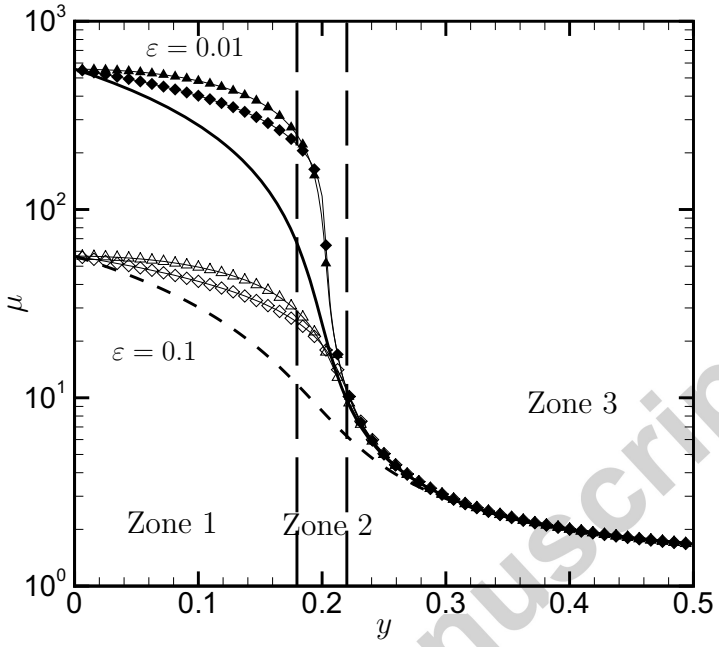

Figure 2: Effective viscosity as a function of y for the different regularized models, with $y_0 = 0.2$, $\varepsilon = 0.1$ and $\varepsilon = 0.01$ ($- - -$ and $\longrightarrow$: simple model, $\triangle$ and $\blacktriangle$: Bercovier model , $\Diamond$ and $\blacklozenge$: Papanastasiou model). The vertical long-dashed lines which bound the transition zone are drawn only to illustrate the different zones and don't characterize the effective thickness δ_y.

$\varepsilon \to 0$. However the effective viscosity, firstly is not defined for the Bingham model in the plug zone, and secondly for the regularized models, it behaves as B/ε near the axis. Actually, the analysis of effective viscosity profile for the regularized models (Fig.(2)) suggests that three zones can be distinguished: the zone 1 around the axis, where $\tau << B$ and for which the effective viscosity is very high. The zone 3 close to the wall, where $\tau >> B$ and for which the effective viscosity is lower than in the previous zone. Finally, the intermediate zone, zone 2, where $\tau \sim B$ and for which the effective viscosity varies drastically.

A characteristic scale δ_y of the intermediate zone thickness is estimated using an asymptotic method. This method is detailed in Appendix A. It consists on determining an approximation of $\dot{\gamma}$ in the regions 1 and 3. Then, approximations can be matched in the zone around $y_0/2$. The results are

Table 1: Asymptotic behaviour of the rate of strain and the thickness of zone 2

	Simple model	Papanastasiou model	Bercovier model
Zone 1: $\tau << B$	$\dot{\gamma}_s \sim \frac{\varepsilon\,\tau}{(B-\tau)}$	$\dot{\gamma}_p \sim -\varepsilon\, ln(1-\frac{\tau}{B})$	$\dot{\gamma}_{be} \sim (\varepsilon^2\tau)^{\frac{1}{3}}$
Zone 2: $\tau \sim B$	$\dot{\gamma}_s \sim \sqrt{\varepsilon B}$	$\dot{\gamma}_p \sim \delta_p \sim -\varepsilon\, ln(1-\frac{\dot{\gamma}_p}{B})$	$\dot{\gamma}_{be} \sim (\varepsilon^2 B)^{\frac{1}{3}}$
Zone thickness: δ_y	$\delta_{y_s} \sim \left(2\frac{y_0}{B}\right)\sqrt{\varepsilon B}$	$\delta_{y_p} \sim \left(2\frac{y_0}{B}\right)\delta_p$	$\delta_{y_{be}} \sim \left(2\frac{y_0}{B}\right)(\varepsilon^2 B)^{\frac{1}{3}}$
Zone 3: $\tau >> B$	$\dot{\gamma}_s \sim \tau - B$	$\dot{\gamma}_p \sim \tau - B$	$\dot{\gamma}_{be} \sim \tau - B$

summarized in Table 1. It is noticeable that the transition zone thickness depends on the model used, moreover for all the models, δ_y increases with ε and B. Moreover, it is noticeable that for ε and B given, we have:
$\delta_{y_p} \leq \delta_{y_{be}} \leq \delta_{y_s}$.

3. Linear stability analysis

The linear stability analysis is developed for the Bingham model in Ref.[2]. For bidimensional perturbations, we introduce the stream function perturbation ψ, defined by $u = \partial_y\psi$ and $v = -\partial_x\psi$, where (u, v) corresponds to the velocity perturbation components. Furthermore, the perturbation solution is seeked in normal mode form as follows:

$$(\psi, T) = (f(y), \theta(y))\, e^{1\alpha(x-ct)} \tag{11}$$

where the parameters α and c are respectively a real axial wave number and a complex wave speed.

Then, the system of linearised perturbation equations writes:
In the two yielded zones, $\frac{1}{2}y_0 <\mid y \mid< \frac{1}{2}$:

$$\mathcal{L}_1 f + Pr\, Ra\, \theta = c\, \mathcal{L}_2 f, \tag{12}$$

$$\mathcal{L}_3\, \theta + f = c\, \theta, \tag{13}$$

where the linear differential operators $\mathcal{L}_1, \mathcal{L}_2$ and $\mathcal{L}_3$ are defined as:

$$\begin{cases} \mathcal{L}_1 \equiv Pr\,Re\,\left[U_b(D^2-\alpha^2) - D^2U_b\right] + i\,\dfrac{Pr}{\alpha}(D^2-\alpha^2)^2 - 4\,i\,\alpha\,Pr\,B\,D\,\left[D\left[FD\right]\right], \\ \mathcal{L}_2 \equiv D^2-\alpha^2, \\ \mathcal{L}_3 \equiv Pr\,Re\,U - i\alpha + \dfrac{i}{\alpha}D^2, \end{cases} \tag{14}$$

In the unyielded zone, $y \in \left[-\dfrac{y_0}{2}, \dfrac{y_0}{2}\right]$ we have:

$$f = 0 \quad \text{and} \quad \mathcal{L}_3\,\theta = c\,\theta. \tag{15}$$

The boundary conditions, in terms of stream function, are:
$f\left(\pm 1/2\right) = f_y\left(\pm 1/2\right) = f\left(\pm y_0/2\right) = f_y\left(\pm y_0/2\right) = 0$ and $\theta\left(\pm 1/2\right) = 0$.

Concerning the regularized models, the linear stability analysis is similar to the one developed in the yielded zone for the previous case. However two fundamental differences remain: (i) the Bingham model leads to zero velocity perturbation at the interface and in the plug zone while the regularized models do not lead to unyielded regions, (ii) compared with the Bingham model, an additional viscous term appears in the Orr-Sommerfeld equation. Finally we get :

$$\left(\mathcal{L}_1 + \mathcal{L}_1^*\right) f + Pr\,Ra\,\theta = c\,\mathcal{L}_2 f\,, \tag{16}$$

$$\mathcal{L}_3\,\theta + f = c\,\theta\,, \tag{17}$$

where: $\mathcal{L}_1^* \equiv -i\,Pr\,B\left[\dfrac{1}{\alpha}\left(D^2+\alpha^2\right)\left(G\left(D^2+\alpha^2\right)\right)\right]$ and $G = F + \dot{\gamma}\dfrac{dF}{d\dot{\gamma}}$.

The boundary conditions are written at walls: $f\left(\pm 1/2\right) = f_y\left(\pm 1/2\right) = 0$ and $\theta\left(\pm 1/2\right) = 0$.

In comparison with the Bingham model, an additional operator $\mathcal{L}_1^*$ appears in Orr-Sommerfeld equation. Actually, this latter induces numerical diverging results due to the function D^2G, since abrupt variations are observed at $y = 0$ and $y = \pm y_0/2$ (Fig.3). For convenience, logarithmic coordinates are adopted, therefore the points for which $D^2G \leq 0$ are not represented.

4. Results and discussion

The discretization of the differential equations set is performed, for the Bingham and the regularized models, by means of a second-order centered

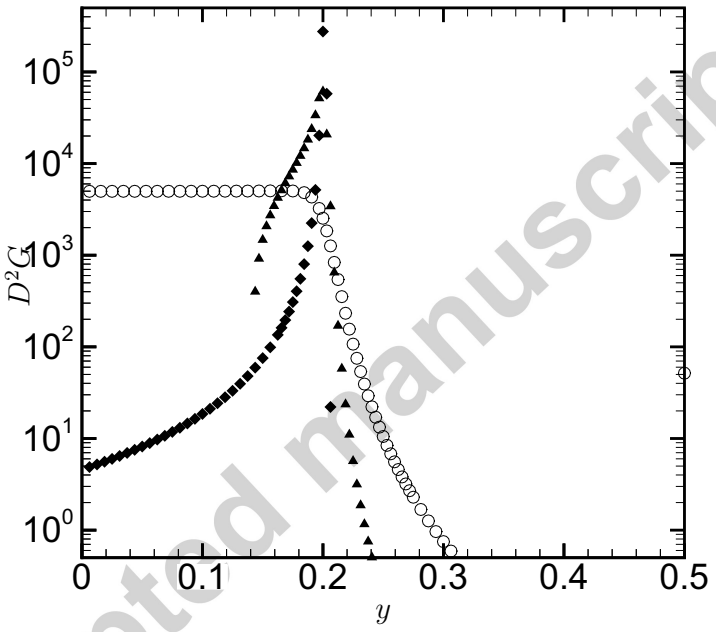

Figure 3: Second derivative of function G for $y_0/2 = 0.2$ ($B = 5.55$), $\varepsilon = 0.01$ ($\circ$: simple model, ▲ : Bercovier model , ♦ : Papanastasiou model)

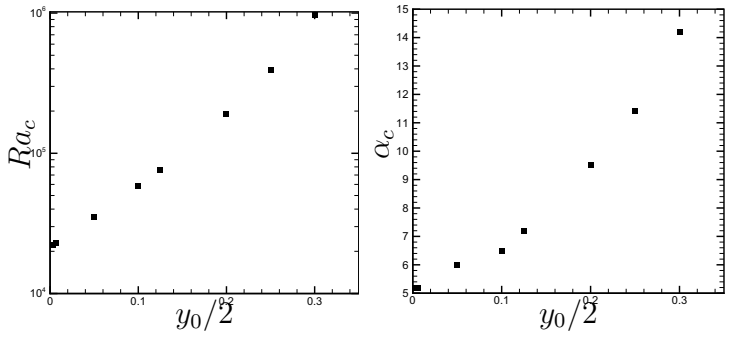

(a) Critical Rayleigh number (b) Critical wave number

Figure 4: Critical conditions as a function of the plug zone width for $Re = 1$, $Pr = 10$: Bingham model

finite difference scheme. A generalized eigenvalues problem is obtained and is solved using QZ algorithm implemented in Matlab 6.5. For numerical validation, we considered the classical Rayleigh-Bénard problem for Newtonian fluid. For 200 nodes, the relative difference between the critical Rayleigh number, Ra_c, obtained in this study and the well known result of 1708 is 0.5%. The results presented in this paper are obtained with 301 nodes.

Concerning the Bingham model, Figs. (4(a)) and (4(b)) give the evolution of the critical conditions, Ra_c and α_c respectively, as a function of y_0, for $Re = 1$ and $Pr = 10$.

These figures highlight the stabilizing effect of the Bingham number. According to [3], this is a consequence of the the unyielded region increasing, in which the velocity perturbation vanishes, as well as the increase in the effective viscosity in the flow domain. When $y_0 \to 0$, there is an outstanding discrepancy, in terms of critical conditions, with those obtained for Newtonian fluids. Métivier *et al.* [2] deal with this particular case. It is shown that the discrepancy is due to the fact that, in the frame of the linear stability analysis, the plug zone remains intact even when $y_0 \to 0$.

When regularized models are used, the abrupt variation of D^2G near the interface generates difficulties in the eigenvalues computation. In this case and similarly to [4], spurious eigenvalues, are obtained as well as incoherent results from physical point of view. In fact, these difficulties increase when the thickness δ_y of the transition zone decreases. In order to improve con-

verging computations, the operator $\mathcal{L}_1^*$ is artificially cancelled and the values of ε are restricted to $\varepsilon \geq 0.01$. The resulting equation can be seen as a regularization of the Orr-Sommerfeld equation.

The regularization of the Orr-Sommerfeld operator leads to spectra shown in Fig. (5). These spectra are obtained at criticality. Preliminary numerical tests have been performed on the resulting spectra by varying N from 201 to 401. Results show that spectra are not modified with N, except some eigenvalues. These eigenvalues are such that $c_i < 0$ and $\min |c_i| = O(10^2)$. In this sense, these spurious values can't be confused with the least stable eigenvalues which are negative and close to 0. According to Fig. (5), one observes that spectra are slightly different comparing each model. Actually, the choice of the model modifies fundamentally the nature of the fluid via its rheological properties comparing to another model. Concerning the Bercovier and Papanastasiou models, one observes that for $\varepsilon = 0.01$, the tendency of spectra are close to the Bingham one. Few modifications are observed using the simple model by varying ε between 0.1 and 0.01.

Concerning critical conditions, Fig. (6) presents the Ra_c values obtained for each model as a function of y_0, for the case $Pr = 10$, $Re = 1$, $\varepsilon = 0.1$ and $\varepsilon = 0.01$. As expected, one observes that considering $y_0 \to 0$, regularized models allow to obtain the critical Rayleigh number corresponding to the Newtonian case, *i.e.* $Ra_{cNew} = 1750$ [10]. In addition, one can observe that the increase in y_0 has a stabilizing effect on the flow field for each model. Indeed, increasing y_0 increases the mean effective viscosity as well as the thickness of zone 1 in which the viscosity is very large. It is also noticeable that the critical conditions obtained with the regularized models can lead to strongly different values from those obtained with the Bingham model. The model leading to the largest difference is the simple model while the Papanastasiou model leads to the smallest difference.

When y_0 is fixed, decreasing ε makes the thickness δ_y smaller and the effective viscosity larger in the zone 1. The increasing effective viscosity tends to stabilize the flow which is in agreement with [3]. Concerning the decrease of δ_y, it seems that it tends to destabilize the flow. The same tendency was indicated in [11]. Figure (6) also shows the effect of ε on Ra_c for the three regularized models. One observes that the variation in ε values do not lead to converging critical conditions since ε modifies the rheological properties of the fluid, in particular the mean viscosity as well as the viscosity stratification in the flow. Actually, the decrease in ε stabilizes the flow for the simple and Papanastasiou models, while it destabilizes the flow for the

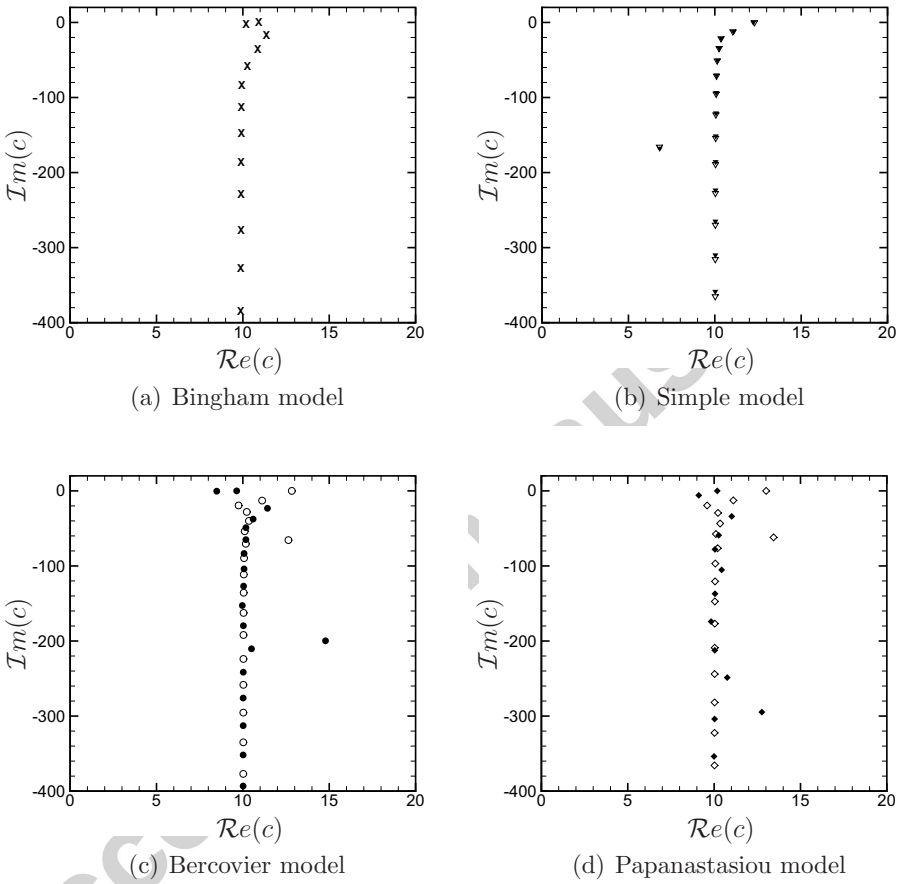

(a) Bingham model (b) Simple model

(c) Bercovier model (d) Papanastasiou model

Figure 5: Spectra obtained at criticality for the regularized models and $y_0/2 = 0.14\, Re = 1$, $Pr = 10$ ($\diamondsuit$: Papanastasiou model ; O: Bercovier model and ∇: Simple model, with $\varepsilon = 0.1$ (white symbols) and $\varepsilon = 0.01$ (black symbols))

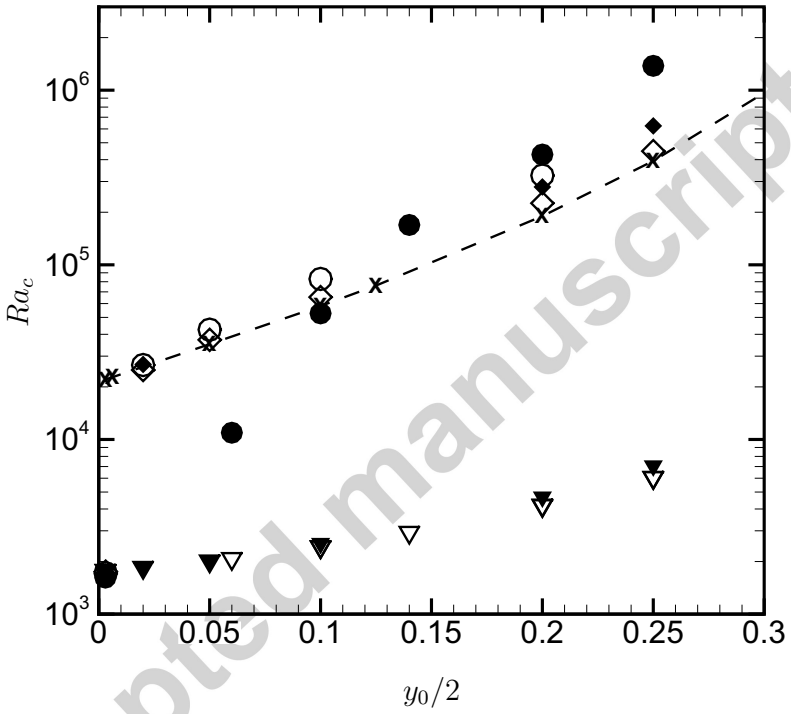

Figure 6: Ra_c versus $y_0/2$ for $Re = 1$, $Pr = 10$ and different values of ε (dashed lines and crosses: Bingham model ; $\diamondsuit$: Papanastasiou model ; O: Bercovier model and ∇: Simple model, with $\varepsilon = 0.1$ (white symbols) and $\varepsilon = 0.01$ (black symbols))

Bercovier model.

The representation of the perturbation modes are given for each regularized model in Fig. (7). One can notice that the stream function has a non zero flat profile in the very high viscosity region (zone 1) considering the simple model, figure 7(a). Furthermore, using the Bercovier and Papanastasiou models, the stream function tends to vanish in this region similarly to the critical modes obtained with the Bingham model as given in Fig. (8).

As a conclusion, the usage of regularized models in instability problems leads to different results according to the chosen model. Indeed, the variation in ε value can modify the rheological properties of the material. In order to obtain physical results, the Orr-Sommerfeld equation has to be regularized, neglecting the ε terms. The comparison between regularized models indicates (i) that these models permit to recover the Newtonian critical conditions for weak values of y_0, (ii) that the Bercovier and Papanastasiou models can tend to similar behaviour as the Bingham case, for $y_0 > O(10^{-1})$ and $\varepsilon = 0.01$. In this last case, same tendencies in spectra and perturbation modes are observed.

Finally, the RBP flow is unstable for both Newtonian and (exact) Bingham cases such as the Taylor-Couette flow. It seems that in such a case, the regularization can tend to the exact Bingham results, when the values of ε are small enough.

Appendix A. Asymptotic analysis for the different regularized models

Appendix A.1. Simple model

Considering first the simple regularized model. This model is described by Eq. (7). Developing it, we get a polynomial equation in power of $\dot{\gamma}_s$:

$$\dot{\gamma_s}^2 + (\varepsilon + B - \tau)\,\dot{\gamma}_s - \varepsilon\,\tau = 0, \tag{A.1}$$

for which the solution is :

$$2\dot{\gamma}_s = +(\tau - \varepsilon - B) + \sqrt{(\varepsilon + B - \tau)^2 + 4\varepsilon\,\tau}. \tag{A.2}$$

In the zone 1, where $\tau << B$, Eq. (A.2) could be expanded as follow:

$$2\dot{\gamma}_s = +(\tau - \varepsilon - B) + (\varepsilon + B - \tau)\left(1 + \frac{2\varepsilon\,\tau}{(\varepsilon + B - \tau)^2}\right) + O(\varepsilon^2). \tag{A.3}$$

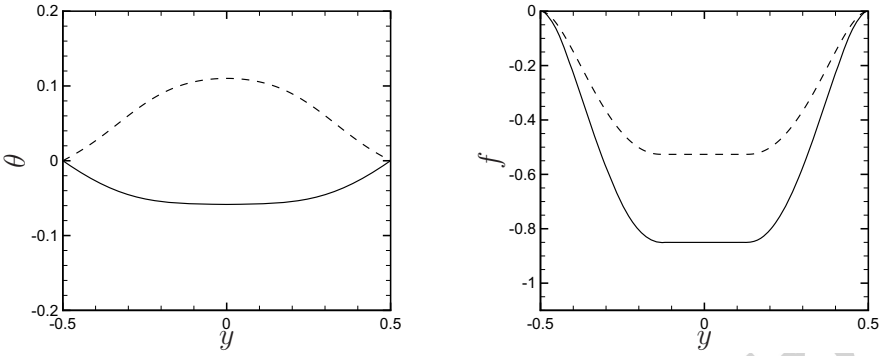

(a) Simple model $\varepsilon = 0.01$

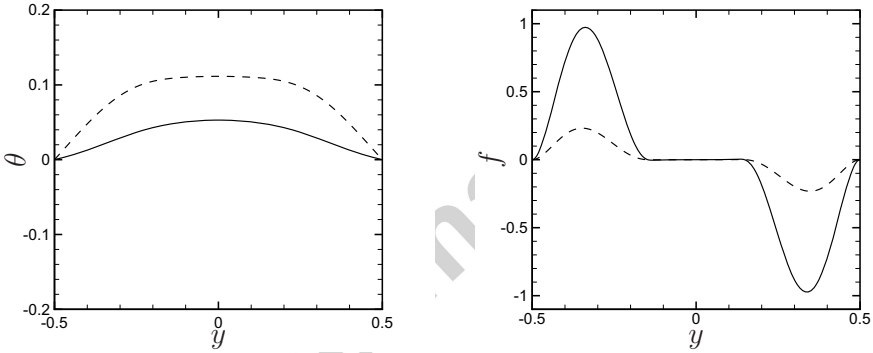

(b) Bercovier model $\varepsilon = 0.01$

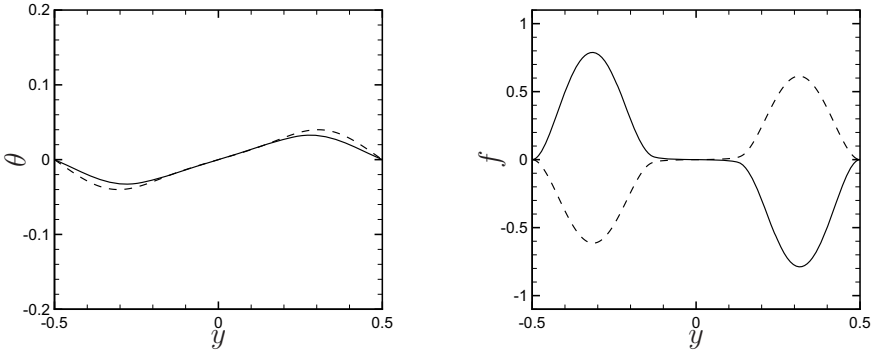

(c) Papanastasiou model $\varepsilon = 0.01$

Figure 7: Critical modes of the perturbation: temperature (left) and stream function (right) (——— : Real part) ; (- - - : Imaginary part) ; $y_0 = 0.14$, $Re = 1$ and $Pr = 10$.

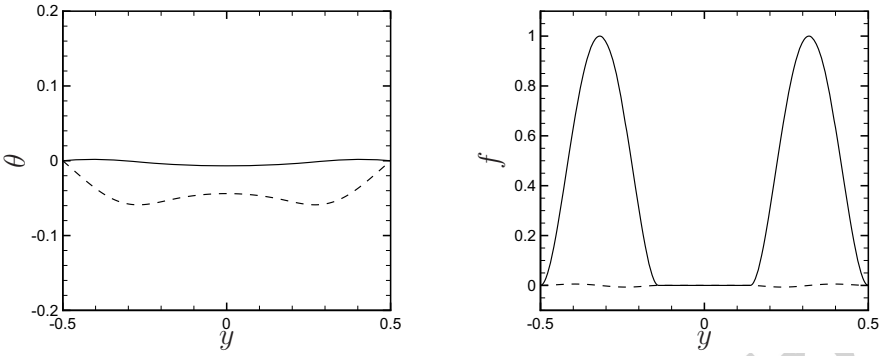

Figure 8: Critical modes of the perturbation in the Bingham case: temperature (left) and stream function (right) (——— : Real part) ; (- - - : Imaginart part) ; $y_0 = 0.14$, $Re = 1$ and $Pr = 10$.

Then, we get:

$$\dot{\gamma}_s = \frac{\varepsilon\,\tau}{(B-\tau)} + O(\varepsilon^2). \tag{A.4}$$

In the zone 3, where $\tau >> B$, Eq. (A.2) could be also written as follow:

$$2\dot{\gamma}_s = +(\tau - \varepsilon - B) + \sqrt{(\varepsilon - B + \tau)^2 + 4\varepsilon\,B}. \tag{A.5}$$

This equation gives asymptotically:

$$2\dot{\gamma}_s = +(\tau - \varepsilon - B) + (\varepsilon - B + \tau)\left(1 + \frac{2\varepsilon\,B}{(\varepsilon - B + \tau)^2}\right) + O(\varepsilon^2). \tag{A.6}$$

Finally we obtain:

$$\dot{\gamma}_s = (\tau - B) + \frac{\varepsilon\,B}{(\tau - B)} + O(\varepsilon^2). \tag{A.7}$$

In the transition zone, where $\tau \sim B$, we write:

$$\tau - B = \delta_s x, \tag{A.8}$$

with $x \in [-1; 1]$. Actually $x = 0$ corresponds to $\tau = B$, *i.e.*, $y = y_0/2$. Moreover, for $x \in [0; 1]$, the solution for $\dot{\gamma}_s$ satisfies:

$$\dot{\gamma}_s \sim \tau - B, \tag{A.9}$$

then

$$\dot{\gamma}_s \sim \delta_s. \tag{A.10}$$

For $x \in [-1;0]$, $\dot{\gamma}_s$ is such that:

$$\dot{\gamma}_s \sim \frac{\varepsilon\tau}{\delta_s} \sim \frac{\varepsilon B}{\delta_s}. \tag{A.11}$$

Finally, we obtain for $x \in [-1;1]$ that:

$$\delta_s \sim \sqrt{\varepsilon B}. \tag{A.12}$$

Appendix A.2. Papanastasiou model

We adopt the same procedure for the Papanastasiou model. In the region 1, where $\tau << B$, we write:

$$\dot{\gamma}_p = -\varepsilon\, ln(1 - \frac{\tau}{B} + \frac{\dot{\gamma}_p}{B}), \tag{A.13}$$

neglecting the term $\frac{\dot{\gamma}_p}{B}$ in the logarithm, we have:

$$\dot{\gamma}_p \sim -\varepsilon\, ln(1 - \frac{\tau}{B}). \tag{A.14}$$

In the zone 3, we consider that the $e^{-\frac{\dot{\gamma}_p}{\varepsilon}}$ is negligible as ε is weak and $\dot{\gamma}_p$ takes finite values. Then:

$$\dot{\gamma}_p \sim \tau - B. \tag{A.15}$$

Considering the transition zone, $\tau \sim B$, the inner solution is not defined close to $y_0/2$. Actually, the term we have neglected is important in this zone. In fact, we have to write for $x \in [-1;0]$:

$$\dot{\gamma}_p \sim -\varepsilon ln(\frac{\dot{\gamma}_p}{B}). \tag{A.16}$$

For $x \in [0;1]$, similarly to previous models, we have:

$$\dot{\gamma}_p \sim \delta_p. \tag{A.17}$$

Finally, for $x \in [-1;1]$, we get:

$$\delta_p \sim -\varepsilon ln(\frac{\delta}{B}). \tag{A.18}$$

Appendix A.3. Bercovier model

Concerning the Bercovier model, we have:

$$\tau \sqrt{\dot{\gamma}_{be}^2 + \varepsilon^2} = \dot{\gamma}_{be} \sqrt{\dot{\gamma}_{be}^2 + \varepsilon^2} + B\, \dot{\gamma}_{be}, \tag{A.19}$$

multiplying this equation by $\sqrt{\dot{\gamma}_{be}^2 + \varepsilon^2}$, we get:

$$(\dot{\gamma}_{be}^2 + \boldsymbol{\varepsilon^2})\, \boldsymbol{\tau} - \boldsymbol{\dot{\gamma}_{be}}(\boldsymbol{\dot{\gamma}_{be}^2} + \varepsilon^2) - B\, \dot{\gamma}_{be} \sqrt{\dot{\gamma}_{be}^2 + \varepsilon^2} = 0. \tag{A.20}$$

In the zone 1, where $\tau << B$, we apply the principle of least degeneration :

$$\dot{\gamma}_{be}^3 \sim \varepsilon^2 \tau, \tag{A.21}$$

then:

$$\dot{\gamma}_{be} \sim (\varepsilon^2 \tau)^{\frac{1}{3}}. \tag{A.22}$$

The zone where $\tau >> B$ concerns the case where $\dot{\gamma}_{be} >> \varepsilon$, then we write:

$$\tau = \dot{\gamma}_{be} + B\,(1 + \frac{\varepsilon^2}{\dot{\gamma}_{be}^2})^{-\frac{1}{2}}, \tag{A.23}$$

$$= \dot{\gamma}_{be} + B\,(1 - \frac{\varepsilon^2}{2\,\dot{\gamma}_{be}^2}) + O(\varepsilon^3) \tag{A.24}$$

Finally, we obtain:

$$\dot{\gamma}_{be} \sim \tau - B. \tag{A.25}$$

The method is similar as previous and permits to lead to:

$$\dot{\gamma}_{be} \sim \delta_{be}, \qquad \text{for } x \in [0; 1], \tag{A.26}$$

$$\dot{\gamma}_{be} \sim (\varepsilon^2 \tau)^{\frac{1}{3}}, \qquad \text{for } x \in [-1; 0]. \tag{A.27}$$

Finally, connecting the solutions, we get:

$$\delta_{be} \sim (\varepsilon^2 \tau)^{\frac{1}{3}}. \tag{A.28}$$

Appendix A.4. Transition zone thickness

At this stage, we know the asymptotical behaviour of each model in the different zones. Moreover, the dimension of the zone in which the viscosity variation is the most important is defined by δ. Indeed, we have:

$$\tau - B \sim 2\delta, \tag{A.29}$$

that we can write in terms of y, replacing τ by its expression:

$$\tau - B = \frac{2B}{y_0}(y - y_0). \tag{A.30}$$

Finally, we introduce a characteristic variable defined as follow:

$$y_{char} = B\frac{y - y_0}{y_0 \times \delta}. \tag{A.31}$$

References

[1] Bird B., Dai G.C., Yarusson B.J., "The rheology and flow of viscoplastic material" *Reviews in Chemical Engineering*, **1** (1983) 1.

[2] Métivier C., Nouar C., Brancher J.P., "Linear stability involving the Bingham model when the yield stress approaches zero," *Phys. Fluids*, **17** 10 (2005).

[3] Métivier C., Nouar C., "On linear stability of Rayleigh-Bénard Poiseuille flow of viscoplastic fluids,," *Phys. Fluids*, **20** 10 (2008).

[4] Frigaard I.A., Nouar C., "On the usage of viscosity regularisation method for visco-plastic fluid flow computation," *J. Non-Newtonian Fluid Mech.*, **127** (2005) 1-26.

[5] Caton F., "Linear stability of circular Couette flow of inelastic viscoplastic fluids," *J. Non-Newtonian Fluid Mech.*, **134** (2006) 148-154.

[6] Govindarajan R., Procaccia I.,Sameen A., "Stabilization of hydrodynamic flows by small viscosity variations", *Physical Review E*, **67** 2, 26310 (2003)

[7] Beris A.N., Tsamopoulos J.A., Armstrong R.C., Brown R.A., "Creeping motion of a sphere through a Bingham plastic" *J. Fluid Mech.*, **158** (1985) 219.

[8] Papanastasiou T.C., "Flows of materials with yield," *J. Rheol.*, **31** (1966) 385.

[9] Bercovier M., Engelman M., "A finite element method for incompressible non-Newtonian flows," *J. Comp. Phys.*, **36** (1980) 313.

[10] Nicolas X., Luijkx J.-M. and Platten J.-K., "Linear stability of mixed convection flows in horizontal rectangular channels of finite transversal extension heated from below.," *Int. J. Heat Mass Transfer*, **43** (2000) 589.

[11] Ern P., Charru F., Luchini P., "Stability analysis of a shear flow with strongly stratified viscosity," *J. Fluid Mech.*, **496** (2003) 295.

Research Highlights:

NLM 1886

Stability of a Rayleigh-Bénard Poiseuille flow for yield stress fluids - Comparison between Bingham and regularized models

by

Christel Métivier and Chérif Nouar

- Comparison between the Bingham and regularized models on the stability of the RBP flow.

- The effective viscosity is not defined in the plug zone for the Bingham model.

- Regularized models lead to the Newtonian critical conditions for weak values of yield stress.

- Convergence of the critical conditions between the simple and the Bingham models is not obtained.

- The Bercovier and Papanastasiou models can tend to the exact Bingham results.